Title

Substrate-Dependent Exciton Diffusion and Annihilation in Chemically Treated MoS2 and WS2

Journal

The Journal of Physical Chemistry C, 124(22)

ISSN

1932-7447

Authors

Goodman, AJ
Lien, D-H
Ahn, GH
et al.

Publication Date

2020-06-04

DOI

10.1021/acs.jpcc.0c04000

Peer reviewed

Substrate Dependent Exciton Diffusion and Annihilation in Chemically Treated MoS_2 and WS_2

A.J. Goodman,[1†] D.-H. Lien,[2†] G.H. Ahn,[2] L.L. Spiegel,[3] M. Amani,[2]
A.P. Willard,[1] A. Javey,[2*] W.A. Tisdale[3*]

1 – Department of Chemistry, Massachusetts Institute of Technology, Cambridge, MA 02139 United States
2 – Department of Electrical Engineering and Computer Science, University of California Berkeley, Berkeley, CA 94720 United States
3 – Department of Chemical Engineering, Massachusetts Institute of Technology, Cambridge, MA 02139 United States
† equal contribution
* to whom correspondence should be addressed (ajavey@mit.edu; tisdale@mit.edu)

ABSTRACT: Atomically thin semiconductors such as monolayer MoS_2 and WS_2 exhibit nonlinear exciton-exciton annihilation at notably low excitation densities (below ~10 excitons/μm^2 in exfoliated MoS_2). Here, we show that the density threshold at which annihilation occurs can be tuned by changing the underlying substrate. When the supporting substrate is changed from SiO_2 to Al_2O_3 or $SrTiO_3$, the rate constant for second-order exciton-exciton annihilation, k_{XX} [cm^2/s], is reduced by one or two orders of magnitude, respectively. Using transient photoluminescence microscopy, we measure the effective room-temperature exciton diffusion coefficient in bis(trifluoromethane)sulfonimide-treated MoS_2 to be in the range D = 0.03-0.06 cm^2/s, corresponding to a diffusion length of L_D = 350 nm for an exciton lifetime of τ = 20 ns, which does not depend strongly on the substrate. We discuss possible mechanisms for the observed behavior, including substrate refractive index, long range exciton-exciton or exciton-charge interactions, defect-mediated Auger recombination, and spatially inhomogeneous exciton populations arising from substrate-induced disorder. Exciton annihilation limits the overall efficiency of 2D semiconductor devices operating at high exciton densities; the ability to tune these interactions via the underlying substrate is an important step toward more efficient optoelectronic technologies featuring atomically thin materials.

KEYWORDS: transition metal dichalcogenides, 2D materials, exciton-exciton annihilation, exciton diffusion, dielectric environment

Since the discovery[1] of monolayer and atomically thin transition metal dichalcogenides (TMDs), the diverse physics of strongly bound and highly absorbing excitons in TMD monolayers has attracted interest in these materials. The dielectric environment resulting from atomically-thin high index media produces anomalous Coulomb interactions[2-4] resulting in stable excitons, trions,[5-6] and biexcitons.[7] Simultaneously, atomically thin optoelectronic devices such as transistors,[8] phototransistors,[9] and LEDs[9-10] have been fabricated. Heterostructures composed of multiple TMDs[11-14] as well as TMDs paired with other complementary nanostructures[4, 15-16] have been explored. Of particular importance for light-emitting applications is the photoluminescence quantum yield (QY). QY values less than unity indicate the presence of non-radiative recombination channels that act to reduce the charge carrier lifetime and limit the brightness of optoelectronic devices. In recent years, a variety of chemical and electrical approaches have been developed that can increase the QY of TMDs.[17-22] These treatments can increase QY at low excitation density, but exciton-exciton annihilation still often limits brightness at device-relevant exciton densities.

Exciton transport and annihilation in TMDs has previously been characterized using a variety of steady state and time-resolved techniques.[23-35] Transient absorption microscopy[26, 36-40] and transient photoluminescence microscopy[28-29, 31, 35, 41] have been particularly powerful approaches, since these techniques allow the spatial extent of the exciton population to be directly visualized. Exciton diffusivities have been reported in the range ~0.1-10 cm^2/s in exfoliated MoS_2, WSe_2 and WS_2.[26-28, 31] However, recent studies on TMDs encapsulated with hexagonal boronitride (hBN)[30, 32, 35] suggest that contributions from the supporting substrate and/or surrounding dielectric environment are responsible for the large spread in reported numbers. Moreover, authors speculate that defects dominate many

experimental observations[26-27, 35] and the interplay between exciton diffusivity, defect states, and exciton-exciton interactions is not clear.

Here, we use time- and spatially-resolved photoluminescence spectroscopy to measure exciton transport and annihilation in bis(trifluoromethane)sulfonimide (TFSI)-treated MoS_2 and WS_2 supported on quartz, sapphire, and strontium titanate (STO). We show that the exciton-exciton annihilation rate constant, k_{XX}, decreases by nearly two orders of magnitude when the substrate is changed from quartz to STO. We directly measure the exciton diffusivity, D, to be 0.06 ± 0.01 cm^2s^{-1} in TFSI-treated MoS_2 using transient PL microscopy, and show that this value does not depend strongly on the substrate. We discuss possible explanations for these contrasting observations and emphasize the importance of suppressing exciton annihilation in optoelectronic devices operating at high exciton densities, including high brightness LEDs, lasers, and polaritonic devices.

Results

MoS_2 and WS_2 monolayers were mechanically exfoliated from bulk single crystals onto SiO_2/Si substrates. The samples were transferred to quartz (amorphous SiO_2, n = 1.45), sapphire (crystalline Al_2O_3, n = 1.76), or strontium titanate ("STO" = crystalline $SrTiO_3$, n = 2.50), substrates chosen for their varied dielectric constant. MoS_2 samples were then encapsulated with a poly(methyl methacrylate) (PMMA) capping layer and treated according to the TFSI treatment detailed by Amani *et al.*[17, 42] The PMMA encapsulation mimics a similar strategy described in the literature by Kim *et al*. that uses fluoropolymer encapsulation to stabilize the TFSI treatment against solvent washing and vacuum exposure.[43] An optical transmission micrograph of an exemplar flake is shown in Fig. 1a and the corresponding substrate/sample/polymer stack is illustrated in Fig. 1b.

Exciton Annihilation Rate

After the TFSI treatment, the PL of the MoS_2 monolayers supported on quartz, sapphire, and STO were markedly enhanced (normalized PL spectra are shown in Fig. 1c, where the peak energies and profiles are identical; corresponding absorption spectra are shown in the supplemental information). Calibrated PL intensity was measured as a function of the generation rate, allowing the extraction of steady-state QYs, which are plotted in Fig. 1d. The QY series for MoS_2 monolayers supported by all three substrates are qualitatively similar; the QY was observed to be near unity at low generation rate and then decreased as the generation rate increased. The QY's dependence on the generation rate can be described by the ratio of the radiative decay rate to the sum of the rates of all decay paths available to the exciton:

$$QY = \frac{k_X N}{k_X N + k_{NR} N + k_{XX} N^2}, \quad (1)$$

where k_X is the radiative decay rate, and k_{NR} and k_{XX} are the first order nonradiative decay rate and the exciton-exciton annihilation rate respectively. This recombination model successfully captures the PL behavior at high generation rate (*i.e.* high laser power) where the QY drops precipitously because exciton-exciton annihilation ($k_{XX}N^2$) begins to outpace radiative decay (k_XN). Note that the QY was near unity in all samples studied at low generation rate, implying that k_{NR} is negligibly small. This allows us to extract k_{XX} = 0.8, 0.02, 0.005 cm^2s^{-1} for the samples on quartz, sapphire, and STO, respectively (the dash lines in Fig 1d are the fits using Eq. 1). Notably, we found that the threshold generation rate at which the QY dropped below 50% could be increased by two orders of magnitude through changing the substrate; for samples on quartz, sapphire, and STO, those generation rates were 1.5×10^{16}, 2.1×10^{17}, and 1.1×10^{18} $cm^{-2}s^{-1}$.

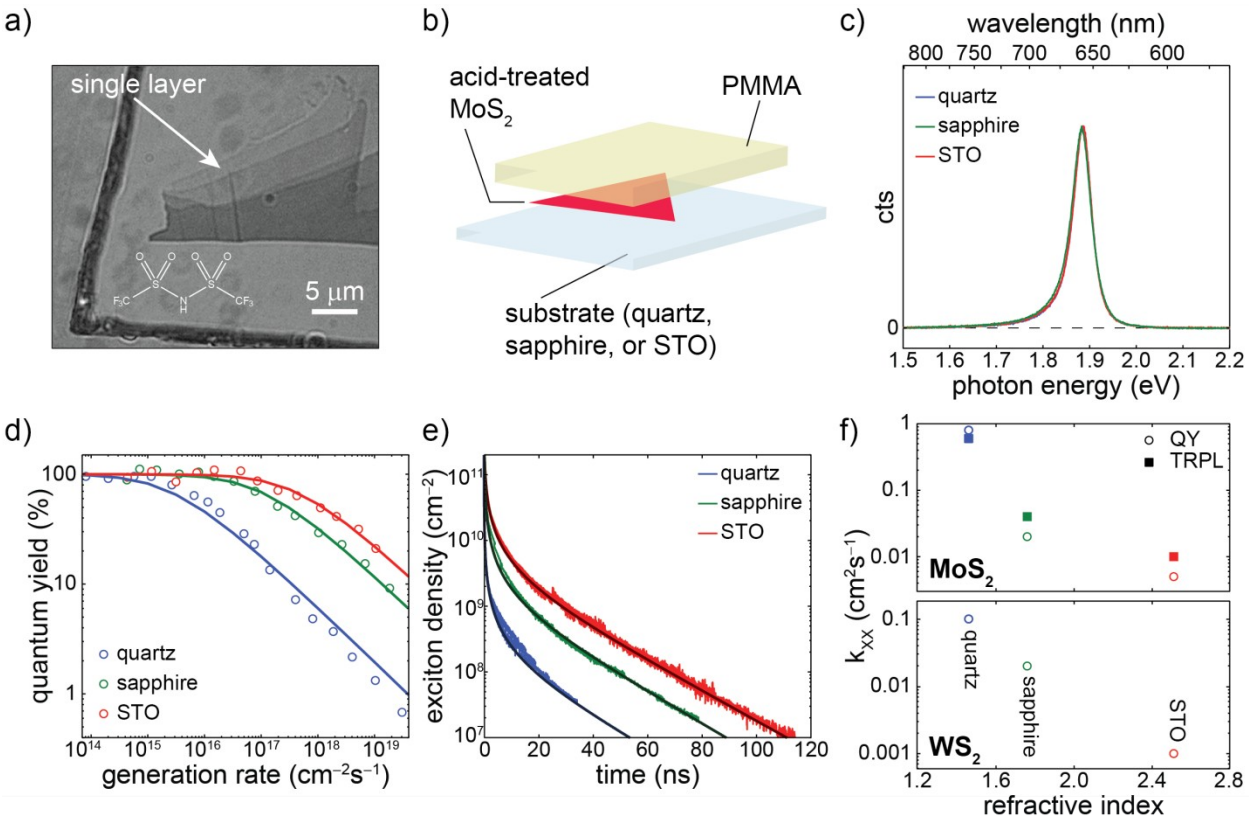

Figure 1 Effect of substrate on photoluminescence. (a) Transmission optical micrograph of exfoliated MoS_2 with monolayer region indicated. The inset depicts the chemical structure of the TFSI used in the treatment. The dark thick line is the border of the polymer capping layer on top of the MoS_2 flake. (b) Schematic of the substrate/MoS_2/polymer stack. (c) Photoluminescence spectra of treated MoS_2 on quartz (blue), sapphire (green), and STO (red). (d) Steady-state QY measured as a function of exciton generation rate. Data were recorded for MoS_2 supported on quartz (blue trace), sapphire (green trace), and strontium titanate (red trace). (e) Time-resolved photoluminescence traces. The traces were globally fit to extract k_X and k_{XX} as described in the text. (f) Exciton-exciton annihilation rate constants, k_{XX}, inferred from steady-state QY measurements (open circles) and time-resolved photoluminescence measurements (filled squares). k_{XX} values for MoS_2 on quartz (blue), sapphire (green), and strontium titanate (red) are plotted against the supporting substrates' refractive indices (top). Analogous data for WS_2 samples are shown in the bottom panel.

The exciton-exciton annihilation rate constant, k_{XX}, can also be extracted from transient measurements. Time correlated single photon counting (TCSPC) measurements were performed at varied incident laser

fluences (corresponding to different initial exciton concentrations, $N(0)$) to reveal recombination dynamics. By stitching together the decay curves with varied $N(0)$, a single decay curve with over 4-decades dynamic range was obtained (individual PL decay curves are provided in the supplemental information). The decay curves for treated MoS_2 supported by all three substrates are shown in Fig. 1e. The decay curves are multiexponential containing fast components due to annihilation at high exciton density and slower radiative decay at low exciton density. The rates k_X and k_{XX} can be extracted by fitting the decay curves to a simple kinetic model, in which the excited exciton density, $N(t)$, decays according to the equation,

$$\frac{dN(t)}{dt} = -k_X N(t) - k_{XX} N^2(t). \quad (2)$$

The values of k_{XX} obtained by this fitting for TCSPC are in good agreement with the values extracted from the steady-state QY measurements, as plotted in the top panel of Fig. 1f. Notably, we observed that k_{XX} varied similarly in WS_2 with changing supporting substrate. The values of k_{XX} found in WS_2 are shown in the bottom panel of Fig. 1f (detail in supplemental information).

Transient Visualization of Exciton Transport

To probe exciton transport, we followed exciton motion in space and time using transient photoluminescence (PL) microscopy.[44] The optical setup is depicted in Fig. 2a. A pulsed laser is focused to a diffraction-limited excitation spot at the sample using an oil-immersion objective, and the epi-fluorescence is collected by the same objective. A 360x magnified image of the fluorescing exciton population is scanned by an APD detector, which is synchronized to the pulsed laser to collect PL decay histograms. A PL decay trace was collected at each detector position in the image plane, allowing time-dependent spatial emission profiles to be reconstructed.

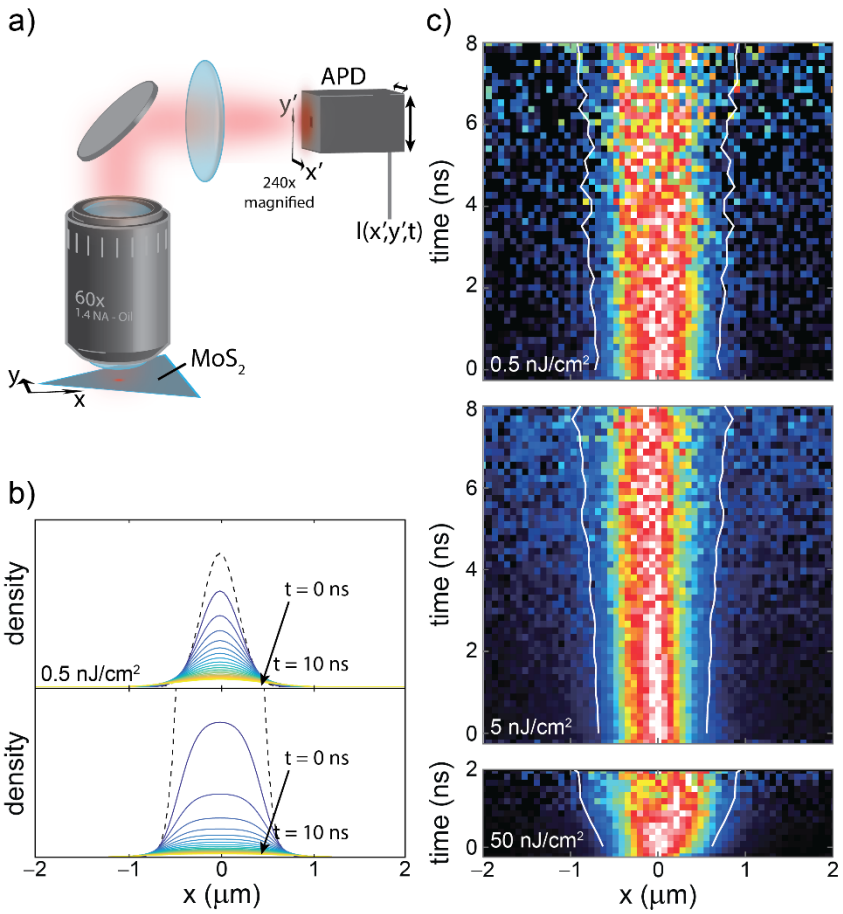

Figure 2 Time- and spatially-resolved emission microscopy. (a) Schematic diagram of the optical apparatus used to resolve exciton diffusion in space and time. (b) top: simulation of the photoluminescence intensity along a line cut of the radially symmetric exciton population as a function time. With an incident fluence of 0.5 nJ/cm^2, almost all excitons decay radiatively and the spot broadens due to diffusion. bottom: same as top panel, but with an incident fluence of 50 nJ/cm^2, many excitons decay due to annihilation. This results in artificial broadening of the density profile; excitons decay most rapidly in the center of the spot where exciton density is highest. (c) Experimentally observed broadening of the exciton population with time at 0.5 nJ/cm^2, 5 nJ/cm^2, and 50 nJ/cm^2 incident fluences in the top, middle, and bottom panels, respectively. White lines indicate the evolution of the standard deviation with time.

The top panel of Fig. 2b depicts the simulated time evolution of an exciton population initialized with a Gaussian spatial profile, indicated by the dashed black trace, designed to mimic the exciton population

instantaneously excited by a 0.5 nJ/cm^2 laser pulse focused to a diffraction limited spot (λ= 405 nm). At this fluence, excitons only decay radiatively. The exciton population decays exponentially as time progresses (coded in the trace colors). Simultaneously, excitons diffuse out of the initial excitation spot, broadening the distribution. We model this decay process in terms of a continuum model in which the exciton density, $N(\boldsymbol{r},t)$, evolves as a function of space and time according to

$$\frac{dN}{dt} = D\nabla^2 N - \left(k_X + k_{NR}\right)N - k_{XX}N^2, \quad (3)$$

where D is the exciton diffusivity. The bottom panel of Fig. 2b depicts an analogous simulation performed with a higher excitation fluence. In this regime, the exciton-exciton annihilation term ($k_{xx}N^2$) in Eq. (3) becomes prominent. Excitons still undergo radiative decay and diffusion, but additionally annihilate with a rate that depends nonlinearly on the local exciton density. The nonradiative decay channel increases the overall decay rate of the exciton population and also changes the shape of the distribution. The peak of the excited distribution decays more quickly than the tails, leading to a flattening and broadening that is not due to diffusion.

In Fig. 2c we present the time-resolved spatial broadening of the exciton population measured in quartz-supported monolayer MoS_2 at three different incident laser fluences. The top panel depicts data collected using a λ = 405 nm excitation fluence of 0.5 nJ/cm^2, corresponding to an average density of 1.2 excitons generated per square micron. The white traces track the standard deviation of the distribution with time. For purely diffusive broadening, the change in the distribution variance grows linearly in time:

$$\sigma^2(t) - \sigma^2(0) = 2Dt. \quad (4)$$

This behavior is observed at low fluences, and fitting the variance as a function of time allows us to extract a diffusivity D_{qtz} = 0.06 ± 0.01 cm^2/s, corresponding to a diffusion length L_D ¿$\sqrt{D\tau}$=¿ 350 nm. In contrast, with higher excitation fluences, the spot appears to broaden more quickly. However, this is due to faster rates of exciton-exciton annihilation in the

center of the distribution rather than faster exciton transport. In these cases, the variance of the intensity distribution $I(x,t)$ grows sublinearly in time. Such details are captured by the data and reproduced by the simulation parameterized by our measured values for k_{XX} and D (see supplemental information). We performed the same measurement for samples supported on sapphire and STO (see supplemental information) and extracted diffusivities $D_{sapphire}$ = 0.04 ± 0.01 cm^2/s and D_{STO} = 0.06 ±0.02 cm^2/s. The choice of substrate did not appear to significantly affect the exciton diffusivity.

Static Visualization of Exciton Transport

To corroborate the time-resolved measurement of exciton diffusivity, we performed a separate measurement of exciton diffusion using steady-state PL microscopy. A λ = 520 nm CW laser was focused to a diffraction limited spot at the sample through an oil immersion objective (NA = 1.4) and the emission was collected through the same objective and imaged on a CCD camera. For CW imaging, the measured emission width is a convolution of 1) the excitation point spread function (PSF) (*i.e.* the Gaussian laser spot size), 2) the collection PSF, and 3) an effective diffusion PSF due to transport during the exciton lifetime. The excitation PSF and collection PSF can be measured independently, allowing the contribution from diffusion to be determined. The collection PSF was assessed by casting a sparse film of isolated CdSe quantum dots (QDs) and imaging their emission (λ_{emiss} = 630 nm) under wide-field LED illumination. Each point-like emitter appeared as a Gaussian spot with a width representing the collection PSF of the imaging system. To measure the excitation PSF, we imaged a homogeneous emissive film that doesn't exhibit exciton diffusion. For these experiments, we used a thin film of CdSe QDs coated with a thick (2-3 nm) ZnCdS shell and long-chain oleate ligands that were previously shown to prevent any measurable exciton diffusion.[45]

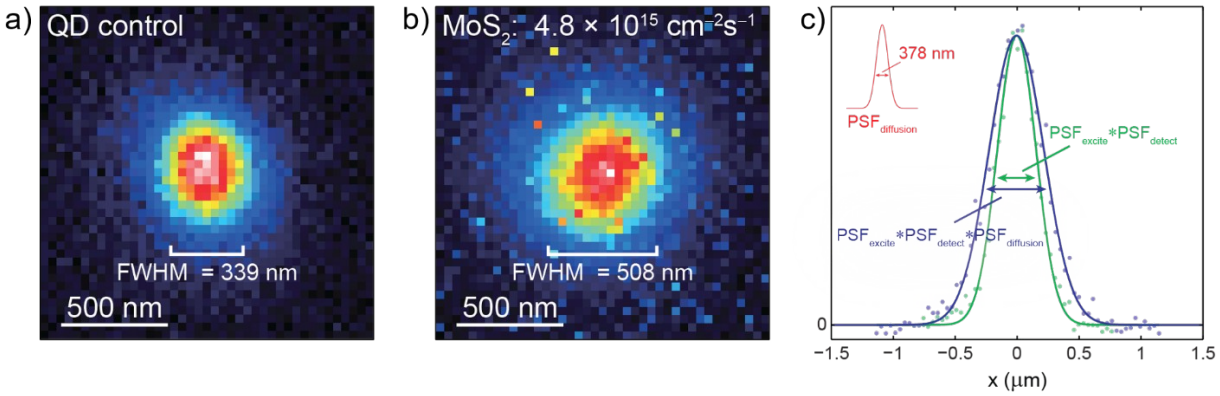

Figure 3 Static emission microscopy. (a) PL image collected from a thin film of well insulated CdSe/ZnCdS core/shell quantum dots in which exciton diffusion doesn't occur. The dots were excited with a focused laser (λ=¿ 520 nm, NA = 1.4). (b) PL image collected from MoS_2 with the same imaging system using a sufficiently low fluence to avoid exciton-exciton annihilation. (c) Radial intensity profiles of the images in the left and center panels, revealing quantifiable broadening in the MoS_2 emission due to exciton diffusion.

A PL image of the QD control sample under focused CW laser excitation is shown in Fig. 3a. The measured width of the emission pattern ($FWHM_{measured}$ = 339 nm) is close to that predicted for a diffraction-limited optical system ($FWHM_{predicted}$ = 304 nm). In Fig. 3b, we show the emission pattern for a TFSI-treated MoS_2 flake on quartz, illuminated with the same focused laser at an excitation rate sufficiently low to avoid exciton annihilation effects (4.8 × 10^{15} cm^{-2} s^{-1}; see Fig. 1d). The MoS_2 emission ($FWHM_{measured}$ = 508 nm) is broadened relative to the QD control due to exciton diffusion in the MoS_2 sample (Fig. 3c). From these measurements, we observe that the variance of the MoS_2 exciton distribution is larger by 0.026 μm^2, implying a diffusivity of 0.03 ± 0.01 cm^2/s, which is consistent with the time-resolved measurements.

Discussion

Exciton Diffusion Constant

The measured low-density exciton diffusivity in TFSI-treated MoS_2, $D \approx$ 0.03-0.06 cm^2/s, which we obtained by two independent methods (transient

imaging and CW imaging – Figs. 2 & 3), is surprisingly small. Exciton diffusivities as large as ~2 cm^2/s have been measured in exfoliated WSe_2[41] and WS_2[26] under much higher laser excitation intensities. The most comparable study is that of Kulig *et al.*, who used transient PL imaging to measure the density-dependent exciton diffusivity in freestanding and SiO_2-supported WS_2 and consistently obtained a value close to 0.3 cm^2/s in the low-density limit.[28] Notably, this value was independent of the presence or absence of the SiO_2/Si substrate, in agreement with our finding that the exciton diffusivity does not depend strongly on the choice of supporting substrate. Nonetheless, the diffusivity we observe in our TFSI-treated samples is at least an order of magnitude smaller than that reported in as-exfoliated flakes.

Comparison of TFSI-treated TMDs to TMDs gated in a capacitor structure strongly suggests that the dominant action of the TFSI treatment is to neutralize majority carriers, thereby preventing fast nonradiative trion recombination.[18] As-exfoliated monolayer MoS_2 is *n*-type because of donor-like chalcogenide site vacancies, whereas TFSI-treated MoS_2 is nearly intrinsic.[17] Upon removal of excess charge carriers – either by chemical treatment[17] or electrical neutralization[18, 22] – luminescence QY approaching 100% can be obtained. Native structural defects are still believed to be present in neutralized TMDs, but these sites do not appear to act as nonradiative recombination centers.

One possible explanation for the smaller-than-expected diffusivity values we measure is the persistent subtle influence of defect sites. Although defects do not limit the luminescence QY, their presence may still impact dynamics of exciton transport, annihilation, and the observed lifetime. Temperature- and density-dependent analysis of the photoluminescence spectrum suggests that, at room temperature, excitons spend a large portion of their lifetime immobilized at defect sites.[46] This could explain the surprisingly small value of the exciton diffusivity that we measure under similar excitation conditions: i.e., the experimentally measured exciton

diffusivity is a time-weighted average of the free and immobile states. The effective diffusivity measured in our experiments is small despite the possibility that excitons diffuse very quickly while at the band edge.

Exciton Annihilation Rate

The central paradox of our data set is the simultaneous observation of very small exciton diffusivity (D = 0.06 cm^2/s on quartz) and very large exciton-exciton annihilation rate constant (k_{XX} = 0.8 cm^2/s on quartz). In quartz-supported MoS_2, the photoluminescence QY dropped to 90% at a generation rate of only 0.5 excitons μm^{-2} per exciton lifetime (τ_X = 20 ns; see Fig. 1d). However, the exciton diffusion length is only L_D = 350 nm.

Exciton-exciton annihilation is usually understood to be a diffusion-mediated process. In the traditional analysis based on Smoluchowski's equation for coagulation of diffusing spheres, excitons are approximated as freely diffusing neutral particles with an effective radius of interaction, R. When two excitons come within a distance $2R$ of each other, one of the excitons is annihilated. The Smoluchowski equation predicts a quantitative relationship between the diffusivity, D, the interaction radius, R, and the annihilation rate constant, k_{XX}. In two dimensions, this equation takes the form,

$$k_{XX} = \frac{8\pi D}{\ln\left(\frac{1}{n_0 4R^2}\right)}, \tag{5}$$

where n_0 is the exciton density at which the annihilation rate becomes equal to the spontaneous decay rate, $k_{XX} n_0^2 = k_X n_0$. According to Equation 5, the annihilation rate constant k_{XX} is proportional to the diffusivity. This is intuitively sensible, since a higher exciton diffusivity leads to more frequent exciton-exciton encounters, resulting in a faster overall annihilation rate.

Using the experimentally measured values of D = 0.06 cm^2/s and k_{XX} = 0.8 cm^2/s on quartz, Equation 5 implies that excitons interact across distances as large as $2R$ = 500 nm. Such a long-range interaction is

inconsistent with current understanding of the exciton size and the strength and distance-dependence of dipole and Coulomb potentials in TMDs. A more reasonable estimate for R is the Bohr radius of the 1s exciton in MoS_2, which has been calculated to be only 5-10 Å.[3, 47] Though the possibility of excitons interacting across hundreds of nanometers is intriguing, it is not likely the correct conclusion to draw from the experimental results.

One possible explanation for the discrepancy between Equation 5 and the measured values of D and k_{XX} is substrate-induced disorder. Roughness of the underlying substrate can induce local strain in a supported TMD, leading to a spatially inhomogeneous bandgap. Strain-induced excitonic energy gradients will drive excitons toward low-energy "pools" where they are more likely to meet and annihilate. This behavior is analogous to exciton transport and annihilation in QD solids, which is strongly influenced by site energy disorder.[45, 48-49] Encapsulation of TMDs in hBN has been shown to suppress exciton-exciton annihilation,[30, 32, 35] partly by protecting the 2D material from substrate-induced disorder.[33]

Another possible explanation for the failure of Equation 5 to predict our experimental results is the presence of long-lived free carriers that persist from the previous excitation event. Though the exciton binding energy in MoS_2 and WS_2 is many times larger than k_bT at room temperature,[2] entropic forces still drive efficient exciton ionization into free carriers[35, 50] – especially at the low excitation densities used here. Free or trapped charges could persist longer than the repetition rate of our pulsed laser (1/40 MHz = 25 ns), leading to a high free carrier density that interacts with the photogenerated exciton population *via* fast trion recombination.

Substrate Dependence

As shown in Fig. 1c, the room-temperature photoluminescence spectrum of MoS_2 was unchanged when the sample was transferred from quartz (n = 1.45) to sapphire (n = 1.76) to STO (n = 2.50). This observation is consistent with theoretical predictions that opposing changes in the

quasiparticle gap and exciton binding energy result in an optical gap that is relatively insensitive to the supporting substrate,[33, 51-52] and is consistent with experimental observations by other groups.[53-54] Moreover, we also found that the first-order decay constant, k_X, remained constant for MoS_2 on all three substrates (see low-density regime of Fig. 1e). This differs from III-V thin film devices in which the radiative recombination rate is highly dependent on the optical mode density and refractive index of the medium.[55]

The optical gap, first-order decay constant, and exciton diffusivity were all unchanged (within experimental precision) when the sample was transferred to different substrates. In contrast, the exciton-exciton annihilation rate constant varied by two orders of magnitude (Fig. 1f). When the substrate was changed from quartz (n = 1.45) to sapphire (n = 1.76) to STO (n = 2.50), the annihilation rate constant monotonically decreased from k_{XX} = 0.8 cm^2/s to 0.02 cm^2/s to 0.005 cm^2/s. Equation 5 predicts a proportionality between k_{XX} and D. Some reduction in the exciton radius of interaction R is expected with increasing substrate refractive index, n, due to environmental screening of the Coulomb and dipole-dipole interaction potentials.[51-52] However, the two-orders-of-magnitude reduction in k_{XX} that was experimentally observed under constant D is more dramatic than Equation 5 can account for.

One clue as to the origin of the substrate-dependent variation in k_{XX} comes from analysis of the emission spectrum at lower temperature. The PL spectrum at 77 K for MoS_2 on all three substrates exhibits a weak tail on the lower-energy side of the dominant exciton emission peak (Fig. S6). The energetic extent of this tail is strongly substrate-dependent, varying monotonically with the substrate refractive index. The lower-index substrate (quartz) exhibits the deepest/most prominent emission tail, whereas the higher-index substrate (STO) exhibits the shallowest/least prominent emission tail. These low energy features correspond to emission from long-lived weakly-radiative states, which we previously assigned to structural defects in the native MoS_2 crystal[46] – presumably chalcogenide site

vacancies. Quantitative analysis of the emission spectrum suggests that the number of defect states per unit area does not depend on the underlying substrate, but that the energetic distribution of defect-associated emission is strongly substrate-dependent (see Supporting Information).

A Model for Defect-Mediated Annihilation

We present a model for defect-mediated annihilation in TMDs. We performed Monte Carlo simulations of exciton transport and annihilation including both mobile and defect-immobilized excitons (see Supporting Information). The results of these simulations, shown in Fig. 4, reproduce most of the experimental observations. Key parameters involving the interaction between trapped and freely diffusing excitons are illustrated in Fig. 4 and summarized in Table S1. In the model, long-lived, immobile trapped excitons or charges act as nonradiative recombination centers for freely diffusing excitons – most likely *via* a defect-mediated Auger recombination process. When diffusing excitons come within a critical radius *R* of a charged defect, they annihilate in a bimolecular process. De-trapping is allowed within the model, but a non-negligible portion of the trapped population does not possess sufficient thermal energy to detrap. This subpopulation of deeply trapped excitons persists for a long time (~microseconds) when compared to the exciton lifetime and the laser repetition rate (10s of ns).[46]

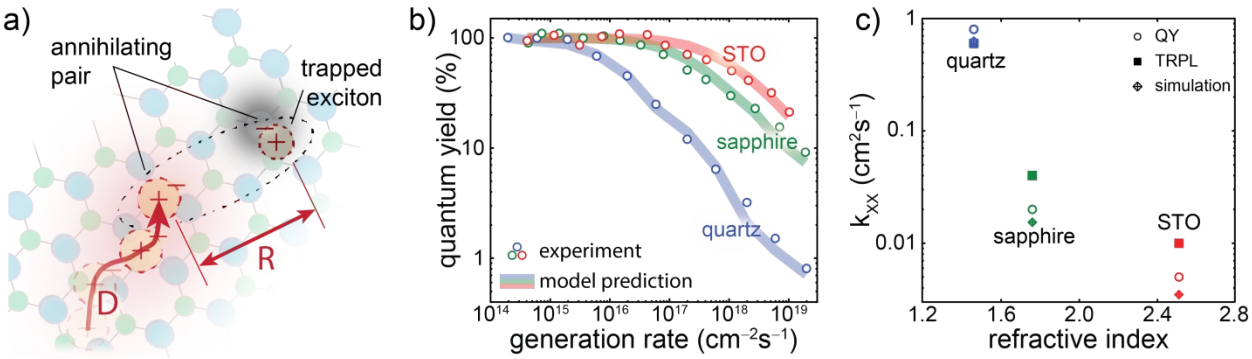

Figure 4 Monte Carlo simulation of defect-mediated annihilation. (a) Diffusing excitons meet long-lived trapped excitons or charges and annihilate according to an interaction radius, *R*. (b) A Monte Carlo model invoking trapped and diffusing band edge excitons quantitatively reproduces steady-state QY data. The simulated behavior is plotted here (thick transparent lines) against the experimental data (open circles) for MoS_2 on quartz (blue), sapphire (green), and strontium titanate (red). (c) The annihilation rate constant inferred from the model (diamonds) is plotted along with the experimentally derived values (open circles, QY; filled squares, time-resolved photoluminescence) against the supporting substrate refractive index.

Within the model framework, the predominant effect of changing substrate is to change the quasi-static charged defect density under equivalent laser irradiation conditions. TFSI treatment removes excess electron density, but does not heal native structural defects. Photogenerated charges can become associated with these defect sites and persist for a long time (~microseconds) relative to time-resolved spectroscopy measurements. Comparison of model simulations to experimental results suggests that the density of defect sites is not changed by TFSI treatment or transfer to different substrates; rather, it is the energetic depth of the trap state distribution that is most affected by the substrate. Higher substrate refractive index is correlated with a shallower trapping depth, thus reducing the fraction of quasi-permanently trapped carriers and allowing near-unity PL QY to be observed experimentally at significantly higher excitation density.

Conclusions

Though TMD lasers[56-57] and LEDs[10, 58-59] have been demonstrated, practical use requires operation at high exciton densities. For instance, a $MoTe_2$ laser[57] exhibited a threshold pump generation rate, $R \approx 4 \times 10^{18}$ $cm^{-2}s^{-1}$, in the regime where exciton-exciton annihilation is dominant. Achieving high brightness LEDs or sufficiently high exciton densities for lasing or polariton condensation in the presence of competitive second order

nonradiative decay channels necessitates excessive pump rates. Exciton-exciton annihilation places a fundamental limit on the operating efficiency of such devices. Understanding the mechanism behind this efficiency loss and raising the maximum achievable operating efficiency by tuning the dielectric environment are critical advances for the future of TMD optoelectronic devices.

Strong exciton-exciton interactions and the tuning of those interactions through the surrounding dielectric are both manifestations of reduced dielectric screening in 2D materials. Coulomb interactions are poorly screened in monolayer TMDs resulting in large exciton, trion, and biexciton binding energies. Though these many-body interactions can be exploited to observe physics characteristic of 2D materials, here they facilitate exciton-exciton and exciton-charge annihilation, limiting radiative efficiency. We take advantage of the sensitivity of exciton dynamics in TMDs to their surrounding dielectric environment to suppress exciton-exciton interactions. Tuning the strength of many-body interactions through the dielectric environment is a powerful design paradigm accessible in low-dimensional materials.

Methods

Sample Preparation – Mineral MoS_2 (SPI) was exfoliated on SiO_2/Si substrates and then transferred to other substrates including quartz, sapphire or STO substrates by a dry transfer technique *via* a polymethyl methacrylate (PMMA) membrane as a transfer media. The transferred MoS_2 was treated by the following procedure: 20 mg of (bis(trifluoromethane)sulfonimide) (TFSI) was dissolved in 5 ml of 1,2-dichloroethane and then diluted with 45 ml 1,2-dichlorobenzene to make a TFSI solution. The transferred MoS_2 with PMMA was then immersed in the TFSI solution for 30 seconds in room temperature. The sample was blow dried with nitrogen. Note that the enhancement is

depending on the initial quality of the sample and only a portion of sample can reach > 95% QY.

Transient PL – Samples were excited using a 405 nm pulsed laser diode (Picoquant, LDH-D-C-405M, 40 MHz repetition rate, 0.4 ns pulse duration) with fluences as indicated in the main text. The laser was focused to a nearly diffraction-limited spot (Nikon, CFI S Plan Fluor ELWD, 40×, 0.6 NA). Fluorescence was collected with the same objective, and passed through a dichroic mirror and 600 nm - 700 nm bandpass filter before being focused onto a Si avalanche photodiode (Micro Photon Devices, PDM50, 50 ps resolution at the detection wavelength). The detector was connected to a counting board for TCSPC (Picoquant, PicoHarp 300). Exciton densities were estimated by relating the photoluminescence rate at time zero with the number of excitons generated by an excitation laser pulse assuming linear absorption and the measured TMD absorption coefficient. The photoluminescence rate was assumed to be proportional to the exciton density (and the radiative rate constant k_X).

Quantum Yield Measurement – The calibrated PL QY measurement has been previously described in detail.[17] Briefly, the 514.5 nm line of an Ar ion laser (Lexel 95) was focused to the sample using a 60× ultra-long working distance objective (NA = 0.7). PL was collected by the same objective, filtered and dispersed by a spectrograph. The emission was detected by a Si CCD camera (Andor, iDus BEX2DD). The excitation power and optical system spectral sensitivity were externally calibrated. The instrument function was cross-calibrated using rhodamine 6G (QY close to 100%) and spectralon as reference samples. The measured PL spectra were integrated and converted into external quantum efficiencies and corresponding QYs. The exciton generation rate was estimated using the measured excitation power, laser spot size, and absorption coefficient at the excitation wavelength.

Transient PL Microscopy – λ=¿ 570 nm pulses from a synchronously pumped optical parametric oscillator (Coherent, PP automatic, 76 MHz, < 1 ps) were

spatially filtered by a single-mode optical fiber and used to excite the sample. The laser was focused to a diffraction-limited spot (Nikon, CFI Plan Apo Lambda, 60× Oil, 1.4 NA). Fluorescence was collected by the same objective and filtered by a dichroic mirror and 600 nm – 700 nm bandpass filter. The APD detector was placed in the 360× magnified image plane outside the microscope. The detector position in the image plane was controlled by two orthogonal motorized actuators (Thorlabs, ZFS25B). The evolution of the photoluminescence spatial profile with time was acquired by scanning the detector across the magnified emission profile and collecting a photoluminescence decay histogram at each position.

PL Spectroscopy, Low Temperature – A 532 nm continuous wave laser (Coherent, Sapphire SF 532-20 CW) was focused at the sample (Nikon, CFI S Plan Fluor ELWD, 40×, 0.6 NA). Fluorescence was collected by the same objective and filtered by a dichroic mirror before being dispersed by a spectrograph (Princeton Instruments, Acton SP2500) and imaged on a cooled CCD camera (Princeton Instruments, Pixis PIX100BR). Low-temperature data were collected under vacuum in a microscope-mounted cryostat (Janis, ST-500-P).

Numerical Simulation – Exciton dynamics were simulated with a fixed time step Monte Carlo algorithm. Excitons were initialized to the band edge according to a spatial profile matching the excitation laser intensity profile. At each time step free excitons hopped a fixed distance in a random direction. Excitons trapped with unit probability if the center position of the exciton was within 0.4 nm of the center of an empty trap. Upon moving within $2R$ nm of an occupied trap, the exciton annihilated and was removed from the simulation. Annihilation between pairs of free excitons were rare due to the low population of detrapped excitons and were thus neglected. Trapped excitons detrapped probabilistically as described in the main text. Detailed procedures and parameter values are included in the Supporting Information file.

Acknowledgements – Transient photoluminescence microscopy and numerical modeling performed at MIT were supported as part of the Center for Excitonics, an Energy Frontier Research Center funded by the US Department of Energy, Office of Science, Basic Energy Sciences (BES) under Award No. DE-SC0001088. Sample preparation and transient PL characterization at U.C. Berkeley was supported by the Electronic Materials Program funded by the Director, Office of Science, Office of Basic Energy Sciences, Materials Sciences and Engineering Division of the U.S. Department of Energy, under contract no. DE-AC02-05Ch11231. A.J.G. acknowledges partial support from the US National Science Foundation Graduate Research Fellowship Program under Grant No. 1122374. W.A.T. was partially supported by the US Department of Energy, Office of Science, under Award No. DE-SC0019345.

Author Contributions – A.J.G. performed time-resolved spectroscopy, diffusion imaging, and low-temperature spectroscopy under the supervision of W.A.T. D.-H.L. prepared samples and performed power-dependent quantum yield and TCSPC experiments under the supervision of A.J. A.J.G. developed and implemented the numerical model, with assistance from L.L.S., A.P.W., and W.A.T. G.H.A. assisted with sample preparation and M.A. contributed to data interpretation. All authors discussed the results and interpretation. W.A.T., A.J.G., and D.-H.L. wrote the manuscript with contributions from the other authors.

Supporting Information –

Supporting information is available in the online version of the paper. Supporting information includes additional experimental results (absorption spectra, data for WS_2, results showing the effect of vacuum and cooling on

the PL spectrum) as well as additional analysis (detailed description of the Monte Carlo model, and fitting of the low-temperature emission spectrum).

Correspondence should be addressed to W.A.T. (tisdale@mit.edu) and A.J (ajavey@berkeley.edu).

Competing Financial Interests – The authors declare no competing financial interests.

References

1. Mak, K. F.; Lee, C.; Hone, J.; Shan, J.; Heinz, T. F., Atomically Thin MoS_2: A New Direct-Gap Semiconductor. *Phys. Rev. Lett.* **2010,** *105*, 136805.
2. Chernikov, A.; Berkelbach, T. C.; Hill, H. M.; Rigosi, A.; Li, Y.; Aslan, O. B.; Reichman, D. R.; Hybertsen, M. S.; Heinz, T. F., Exciton Binding Energy and Nonhydrogenic Rydberg Series in Monolayer WS_2. *Phys. Rev. Lett.* **2014,** *113*, 076802.
3. Mayers, Z. M.; Berkelbach, T. C.; Hybertsen, M. S.; Reichman, D. R., Binding Energies and Spatial Structures of Small Carrier Complexes in Monolayer Transition-Metal Dichalcogenides via Diffusion Monte Carlo. *Physical Review B* **2015,** *92*, 161404.
4. Raja, A.; Montoya-Castillo, A.; Zultak, J.; Zhang, X.-X.; Ye, Z.; Roquelet, C.; Chenet, D. A.; van der Zande, A. M.; Huang, P.; Jockusch, S.; Hone, J. C.; Reichman, D. R.; Brus, L. E.; Heinz, T. F., Energy Transfer from Quantum Dots to Graphene and MoS_2: The Role of Absorption and Screening in Two-Dimensional Materials. *Nano Letters* **2016,** *16* (4), 2328-2333.
5. Mak, K. F.; He, K.; Lee, C.; Lee, G. H.; Hone, J.; Heinz, T. F.; Shan, J., Tightly Bound Trions in Monolayer MoS_2. *Nature Materials* **2013,** *12*, 207-211.
6. Zhang, C.; Wang, H.; Chan, W.; Manolatou, C.; Rana, F., Absorption of Light by Excitons and Trions in Monolayers of Metal Dichalcogenide MoS_2: Experiments and Theory. *Physical Review B* **2014,** *89*.
7. You, Y.; Zhang, X.-X.; Berkelbach, T. C.; Hybertsen, M. S.; Reichman, D. R.; Heinz, T. F., Observation of Biexcitons in Monolayer WSe_2. *Nature Physics* **2015,** *11*, 477-481.
8. Radisavljevic, B.; Radenovic, A.; Brivio, J.; Giacometti, V.; Kis, A., Single-Layer MoS_2 Transistors. *Nat. Nanotechnol.* **2011,** *6*, 147-150.
9. Baugher, B. W. H.; Churchill, H. O. H.; Yang, Y.; Jarillo-Herrero, P., Optopelectronic Devices Based on Electrically Tunable p-n Diodes in a Monolayer Dichalcogenide. *Nat. Nanotechnol.* **2014,** *9*, 262-267.

10. Ross, J. S.; Klement, P.; Jones, A. M.; Ghimire, N. J.; Yan, J.; Mandrus, D. G.; Taniguchi, T.; Watanabe, K.; Kitamura, K.; Yao, W.; Cobden, D. H.; Xu, X., Electrically Tunable Excitonic Light-Emitting Diodes Based on Monolayer WSe_2 p-n Junctions. *Nat. Nanotechnol.* **2014,** *9*, 268-272.
11. Fang, H.; Battaglia, C.; Carraro, C.; Nemsak, S.; Ozdol, B.; Kang, J. S.; Bechtel, H. A.; Desai, S. B.; Kronast, F.; Unal, A. A.; Conti, G.; Conlon, C.; Palsson, G. K.; Martin, M. C.; Minor, A. M.; Fadley, C. S.; Yablonovitch, E.; Maboudian, R.; Javey, A., Strong Interlayer Coupling in van der Waals Heterostructures Built from Single-Layer Chalcogenides. *PNAS* **2014,** *111*, 6198-6202.
12. Hong, X.; Kim, J.; Shi, S.-F.; Zhang, Y.; Jin, C.; Sun, Y.; Tongay, S.; Wu, J.; Zhang, Y.; Wang, F., Ultrafast Charge Transfer in Atomically Thin MoS_2/WS_2 Heterostructures. *Nat. Nanotechnol.* **2014,** *9*, 682-686.
13. Gong, Y.; Lin, J.; Wang, X.; Shi, G.; Lei, S.; Lin, Z.; Zou, X.; Ye, G.; Vajtai, R.; Yakobson, B. I.; Terrones, H.; Terrones, M.; Tay, B. K.; Lou, J.; Pantelides, S. T.; Liu, Z.; Zhou, W.; Ajayan, P. M., Vertical and in-Plane Heterostructures from WS_2/MoS_2 Monolayers. *Nature Materials* **2014,** *13*, 1135-1142.
14. Ma, Q.; Andersen, T. I.; Nair, N. L.; Gabor, N. M.; Massicotte, M.; Lui, C. H.; Young, A. F.; Fang, W.; Watanabe, K.; Taniguchi, T.; Kong, J.; Gedik, N.; Koppens, F. H. L.; Jarillo-Herrero, P., Tuning Ultrafast Electron Thermalization Pathways in a van der Waals Heterostructure. *Nature Physics* **2016,** *12*, 455-459.
15. Prins, F.; Goodman, A. J.; Tisdale, W. A., Reduced Dielectric Screening and Enhanced Energy Transfer in Single- and Few-Layer MoS2. *Nano Letters* **2014,** *14* (11), 6087-6091.
16. Prasai, D.; Klots, A. R.; Newaz, A.; Niezgoda, J. S.; Orfield, N. J.; Escobar, C. A.; Wynn, A.; Efimov, A.; Jennings, G. K.; Rosenthal, S. J.; Bolotin, K. I., Electrical Control of near-Field Energy Transfer between Quantum Dots and Two-Dimensional Semiconductors. *Nano Letters* **2015**.
17. Amani, M.; Lien, D.-H.; Kiriya, D.; Xiao, J.; Azcatl, A.; Noh, J.; Madhvapathy, S. R.; Addou, R.; KC, S.; Dubey, M.; Cho, K.; Wallace, R. M.; Lee, S.-C.; He, J.-H.; Ager III, J. W.; Zhang, X.; Yablonovitch, E.; Javey, A., Near-Unity Photoluminescence Quantum Yield in MoS_2. *Science* **2015,** *350* (6264), 1065-1068.
18. Lien, D.-H.; Uddin, S. Z.; Yeh, M.; Amani, M.; Kim, H.; Ager, J. W.; Yablonovitch, E.; Javey, A., Electrical suppression of all nonradiative recombination pathways in monolayer semiconductors. *Science* **2019,** *364* (6439), 468.
19. Tanoh, A. O. A.; Alexander-Webber, J.; Xiao, J.; Delport, G.; Williams, C. A.; Bretscher, H.; Gauriot, N.; Allardice, J.; Pandya, R.; Fan, Y.; Li, Z.; Vignolini, S.; Stranks, S. D.; Hofmann, S.; Rao, A., Enhancing Photoluminescence and Mobilities in WS2 Monolayers with Oleic Acid Ligands. *Nano Letters* **2019,** *19* (9), 6299-6307.

20. Peimyoo, N.; Yang, W.; Shang, J.; Shen, X.; Wang, Y.; Yu, T., Chemically Driven Tunable Light Emission of Charged and Neutral Excitons in Monolayer WS2. *ACS Nano* **2014,** *8* (11), 11320-11329.
21. Mouri, S.; Miyauchi, Y.; Matsuda, K., Tunable Photoluminescence of Monolayer MoS2 via Chemical Doping. *Nano Letters* **2013,** *13* (12), 5944-5948.
22. Atallah, T. L.; Wang, J.; Bosch, M.; Seo, D.; Burke, R. A.; Moneer, O.; Zhu, J.; Theibault, M.; Brus, L. E.; Hone, J.; Zhu, X. Y., Electrostatic Screening of Charged Defects in Monolayer MoS2. *The Journal of Physical Chemistry Letters* **2017,** *8* (10), 2148-2152.
23. Shi, H.; Yan, R.; Bertolazzi, S.; Brivio, J.; Gao, B.; Kis, A.; Jena, D.; Xing, H. G.; Huang, L., Exciton Dynamics in Suspended Monolayer and Few-Layer MoS_2 2D Crystals. *ACS Nano* **2013,** *7* (2).
24. Yuan, L.; Huang, L., Exciton Dynamics and Annihilation in WS_2 2D Semiconductors. *Nanoscale* **2015,** *7*, 7402-7408.
25. Sun, D.; Rao, Y.; Reider, G. A.; Chen, G.; You, Y.; Brézin, L.; Harutyunyan, A. R.; Heinz, T. F., Observation of Rapid Exciton–Exciton Annihilation in Monolayer Molybdenum Disulfide. *Nano Letters* **2014,** *14* (10), 5625-5629.
26. Yuan, L.; Wang, T.; Zhu, T.; Zhou, M.; Huang, L., Exciton Dynamics, Transport, and Annihilation in Atomically Thin Two-Dimensional Semiconductors. *The Journal of Physical Chemistry Letters* **2017,** *8* (14), 3371-3379.
27. Kato, T.; Kaneko, T., Transport Dynamics of Neutral Excitons and Trions in Monolayer WS2. *ACS Nano* **2016,** *10* (10), 9687-9694.
28. Kulig, M.; Zipfel, J.; Nagler, P.; Blanter, S.; Schüller, C.; Korn, T.; Paradiso, N.; Glazov, M. M.; Chernikov, A., Exciton Diffusion and Halo Effects in Monolayer Semiconductors. *Phys. Rev. Lett.* **2018,** *120* (20), 207401.
29. Onga, M.; Zhang, Y.; Ideue, T.; Iwasa, Y., Exciton Hall effect in monolayer MoS2. *Nature Materials* **2017,** *16* (12), 1193-1197.
30. Cadiz, F.; Robert, C.; Courtade, E.; Manca, M.; Martinelli, L.; Taniguchi, T.; Watanabe, K.; Amand, T.; Rowe, A. C. H.; Paget, D.; Urbaszek, B.; Marie, X., Exciton diffusion in WSe2 monolayers embedded in a van der Waals heterostructure. *Applied Physics Letters* **2018,** *112* (15), 152106.
31. Cordovilla Leon, D. F.; Li, Z.; Jang, S. W.; Cheng, C.-H.; Deotare, P. B., Exciton transport in strained monolayer WSe2. *Applied Physics Letters* **2018,** *113* (25), 252101.
32. Fu, Y.; He, D.; He, J.; Bian, A.; Zhang, L.; Liu, S.; Wang, Y.; Zhao, H., Effect of Dielectric Environment on Excitonic Dynamics in Monolayer WS2. *Advanced Materials Interfaces* **2019,** *6* (23), 1901307.
33. Raja, A.; Waldecker, L.; Zipfel, J.; Cho, Y.; Brem, S.; Ziegler, J. D.; Kulig, M.; Taniguchi, T.; Watanabe, K.; Malic, E.; Heinz, T. F.; Berkelbach, T. C.;

Chernikov, A., Dielectric disorder in two-dimensional materials. *Nat. Nanotechnol.* **2019,** *14* (9), 832-837.

34. Wang, J.; Guo, Y.; Huang, Y.; Luo, H.; Zhou, X.; Gu, C.; Liu, B., Diffusion dynamics of valley excitons by transient grating spectroscopy in monolayer WSe2. *Applied Physics Letters* **2019,** *115* (13), 131902.
35. Zipfel, J.; Kulig, M.; Perea-Causín, R.; Brem, S.; Ziegler, J. D.; Rosati, R.; Taniguchi, T.; Watanabe, K.; Glazov, M. M.; Malic, E.; Chernikov, A., Exciton diffusion in monolayer semiconductors with suppressed disorder. *arXiv* **2019**, 1911.02909.
36. Kumar, N.; Cui, Q.; Ceballos, F.; He, D.; Wang, Y.; Zhao, H., Exciton Diffusion in Monolayer and Bulk $MoSe_2$. *Nanoscale* **2014,** *6*.
37. Kumar, N.; He, J.; He, D.; Wang, Y.; Zhao, H., Charge Carrier Dynamics in Bulk MoS_2 Crystal Studied by Transient Absorption Microscopy. *J. Appl. Phys.* **2013,** *113*.
38. Cui, Q.; Ceballos, F.; Kumar, N.; Zhao, H., Transient Absorption Microscopy of Monolayer and Bulk WSe2. *ACS Nano* **2014,** *8* (3), 2970-2976.
39. Zhu, T.; Yuan, L.; Zhao, Y.; Zhou, M.; Wan, Y.; Mei, J.; Huang, L., Highly mobile charge-transfer excitons in two-dimensional WS2/tetracene heterostructures. *Science Advances* **2018,** *4* (1), eaao3104.
40. Wang, R.; Ruzicka, B. A.; Kumar, N.; Bellus, M. Z.; Chiu, H.-Y.; Zhao, H., Ultrafast and Spatially Resolved Studies of Charge Carriers in Atomically Thin Molybdenum Disulfide. *Phys. Rev. B* **2012,** *86*.
41. Mouri, S.; Miyauchi, Y.; Toh, M.; Zhao, W.; Eda, G.; Matsuda, K., Nonlinear Photoluminescence in Atomically Thin Layered WSe_2 Arising from Diffusion-Assisted Exciton-Exciton Annihilation. *Phys. Rev. B* **2014,** *90*.
42. Amani, M.; Taheri, P.; Addou, R.; Ahn, G. H.; Kiriya, D.; Lien, D.-H.; Ager, J. W.; Wallace, R. M.; Javey, A., Recombination Kinetics and Effects of Superacid Treatment in Sulfur- and Selenium-Based Transition Metal Dichalcogenides. *Nano Letters* **2016,** *16* (4), 2786-2791.
43. Kim, H.; Lien, D.-H.; Amani, M.; Ager, J. W.; Javey, A., Highly Stable Near-Unity Photoluminescence Yield in Monolayer MoS2 by Fluoropolymer Encapsulation and Superacid Treatment. *ACS Nano* **2017,** *11* (5), 5179-5185.
44. Akselrod, G. M.; Deotare, P. B.; Thompson, N. J.; Lee, J.; Tisdale, W. A.; Baldo, M. A.; Menon, V. M.; Bulovic, V., Visualization of exciton transport in ordered and disordered molecular solids. *Nature Communications* **2014,** *5*, 3646.
45. Akselrod, G. M.; Prins, F.; Poulikakos, L. V.; Lee, E. M. Y.; Weidman, M. C.; Mork, A. J.; Willard, A. P.; Bulovic, V.; Tisdale, W. A., Subdiffusive Exciton Transport in Quantum Dot Solids. *Nano Letters* **2014,** *14*, 3556-3562.

46. Goodman, A. J.; Willard, A. P.; Tisdale, W. A., Exciton trapping is responsible for the long apparent lifetime in acid-treated MoS2. *Physical Review B* **2017,** *96* (12), 121404.
47. Ugeda, M. M.; Bradley, A. J.; Shi, S.-F.; da Jornada, F. H.; Zhang, Y.; Qiu, D. Y.; Ruan, W.; Mo, S.-K.; Hussain, Z.; Shen, Z.-X.; Wang, F.; Louie, S. G.; Crommie, M. F., Giant bandgap renormalization and excitonic effects in a monolayer transition metal dichalcogenide semiconductor. *Nature Materials* **2014,** *13* (12), 1091-1095.
48. Lee, E. M. Y.; Tisdale, W. A.; Willard, A. P., Can Disorder Enhance Incoherent Exciton Diffusion? *Journal of Physical Chemistry B* **2015,** *119* (30), 9501-9509.
49. Gao, Y. A.; Sandeep, C. S. S.; Schins, J. M.; Houtepen, A. J.; Siebbeles, L. D. A., Disorder strongly enhances Auger recombination in conductive quantum-dot solids. *Nature Communications* **2013,** *4*, 2329.
50. Gélvez-Rueda, M. C.; Hutter, E. M.; Cao, D. H.; Renaud, N.; Stoumpos, C. C.; Hupp, J. T.; Savenije, T. J.; Kanatzidis, M. G.; Grozema, F. C., Interconversion between Free Charges and Bound Excitons in 2D Hybrid Lead Halide Perovskites. *The Journal of Physical Chemistry C* **2017,** *121* (47), 26566-26574.
51. Cho, Y.; Berkelbach, T. C., Environmentally sensitive theory of electronic and optical transitions in atomically thin semiconductors. *Physical Review B* **2018,** *97* (4), 041409.
52. Steinhoff, A.; Wehling, T. O.; Rösner, M., Frequency-dependent substrate screening of excitons in atomically thin transition metal dichalcogenide semiconductors. *Physical Review B* **2018,** *98* (4), 045304.
53. Li, Y.; Chernikov, A.; Zhang, X.; Rigosi, A.; Hill, H. M.; van der Zande, A. M.; Chenet, D. A.; Shih, E.-M.; Hone, J.; Heinz, T. F., Measurement of the optical dielectric function of monolayer transition-metal dichalcogenides: MoS_2, $MoSe_2$, WS_2, and WSe_2. *Physical Review B* **2014,** *90* (20), 205422.
54. Lin, Y.; Ling, X.; Yu, L.; Huang, S.; Hsu, A. L.; Lee, Y.-H.; Kong, J.; Dresselhaus, M. S.; Palacios, T., Dielectric Screening of Excitons and Trions in Single-Layer MoS2. *Nano Letters* **2014,** *14* (10), 5569-5576.
55. Yablonovitch, E.; Gmitter, T. J.; Bhat, R., Inhibited and Enhanced Spontaneous Emission from Optically Thin AlGaAs/GaAs Double Heterostructures. *Phys. Rev. Lett.* **1988,** *61* (22), 2546-2549.
56. Wu, S.; Buckley, S.; Schaibley, J. R.; Feng, L.; Yan, J.; Mandrus, D. G.; Hatami, F.; Yao, W.; Vuckovic, J.; Majumdar, A.; Xu, X., Monolayer semiconductor nanocavity lasers with ultralow thresholds. *Nature* **2015,** *520* (7545), 69-72.
57. Li, Y.; Zhang, J.; Huang, D.; Sun, H.; Fan, F.; Feng, J.; Wang, Z.; Ning, C. Z., Room-temperature continuous-wave lasing from monolayer molybdenum ditelluride integrated with a silicon nanobeam cavity. *Nat. Nanotechnol.* **2017,** *12* (10), 987-992.

58. Sundaram, R. S.; Engel, M.; Lombardo, A.; Krupke, R.; Ferrari, A. C.; Avouris, P.; Steiner, M., Electroluminescence in Single Layer MoS2. *Nano Letters* **2013,** *13* (4), 1416-1421.
59. Ye, Y.; Ye, Z.; Gharghi, M.; Zhu, H.; Zhao, M.; Wang, Y.; Yin, X.; Zhang, X., Exciton-dominant electroluminescence from a diode of monolayer MoS2. *Applied Physics Letters* **2014,** *104* (19), 193508.

TOC Graphic: